

# Monolithically Integrated Label-Free Optical Immunosensors <sup>†</sup>

Panagiota Petrou <sup>1,\*</sup>, Eleni Makarona <sup>2</sup> , Ioannis Raptis <sup>2</sup>, Sotirios Kakabakos <sup>1</sup>  and Konstantinos Misiakos <sup>2</sup>

<sup>1</sup> Immunoassays/Immunosensors Lab, Institute of Nuclear & Radiological Sciences & Technology, Energy & Safety, National Centre for Scientific Research “Demokritos”, 15341 Aghia Paraskevi, Greece; skakab@rrp.demokritos.gr

<sup>2</sup> Institute of Nanoscience and Nanotechnology, National Centre for Scientific Research “Demokritos”, 15341 Aghia Paraskevi, Greece; e.makarona@inn.demokritos.gr (E.M.); i.raptis@inn.demokritos.gr (I.R.); k.misiakos@inn.demokritos.gr (K.M.)

\* Correspondence: ypetrou@rrp.demokritos.gr; Tel.: +30-2106503819

<sup>†</sup> Presented at the 2nd International Electronic Conference on Biosensors, 14–18 February 2022; Available online: <https://sciforum.net/event/IECB2022>.

**Abstract:** Amongst label-free optical sensors, those relying on silicon photonics are especially promising for the development of small-sized devices appropriate for applications at the point-of-need. In this context, our work over the last 10 years has focused on the development of silicon photonic chips that combine all optical components, both active and passive, onto the same substrate. The approach followed for this monolithic integration, as well as the application of the different silicon photonic chip versions as immunosensors for the determination of single or panels of analytes, related to biodiagnostics or the food safety sector, will be presented.

**Keywords:** optical sensors; label-free detection; monolithic integration; biodiagnostics; food analysis



**Citation:** Petrou, P.; Makarona, E.; Raptis, I.; Kakabakos, S.; Misiakos, K. Monolithically Integrated Label-Free Optical Immunosensors. *Eng. Proc.* **2022**, *16*, 11. <https://doi.org/10.3390/IECB2022-12283>

Academic Editors: Giovanna Marrazza and Sara Tombelli

Published: 15 February 2022

**Publisher’s Note:** MDPI stays neutral with regard to jurisdictional claims in published maps and institutional affiliations.



**Copyright:** © 2022 by the authors. Licensee MDPI, Basel, Switzerland. This article is an open access article distributed under the terms and conditions of the Creative Commons Attribution (CC BY) license (<https://creativecommons.org/licenses/by/4.0/>).

## 1. Introduction

Biosensors have been the subject of intensive research effort aiming to overcome the limitations of classical analytical systems and provide solutions for on-site determinations for more than 50 years, since the first report of Clark and Lyons [1]. As a result, an enormous variety of biosensing principles has been developed, most of which fall into one of the following categories: mass-sensitive, electrochemical, or optical sensors.

Optical biosensors are less vulnerable compared to mass-sensitive and electrochemical ones to interferences from sample components, parasitic electrical signals, and fluctuations in temperature, and therefore more suitable for point-of-need applications. In addition, with respect to electrochemical ones, optical biosensors have the inherent advantage of reduced crossover signals, enabling their application to the simultaneous detection of multiple analytes (multiplexed determinations), which is of high value for fields such as biodiagnostics and food analysis [2–4].

Independently of the transduction principle, biosensors can be also divided into two categories depending on whether or not they implement labels for analyte determination. Despite the fact that optical biosensors employing labels are considered, in general, more sensitive than the label-free ones [5], they are more suited for laboratory rather than point-of-need applications due to the size and complexity of the relative instrumentation. On the other hand, label-free biosensors have also been improved, especially regarding their analytical performance and detection sensitivity, which reaches in many cases that of biosensors employing labels [2–4], as result of the progress made in the last two decades in the field of nanotechnology.

In general, label-free sensors produce a signal when the analyte binds to the specific recognition molecule that has been immobilized onto the transducer surface, thus enabling the real-time monitoring of the binding reaction. This feature allows the performance of

kinetic measurements and, usually, leads to faster assays than the label-based sensing methods. The optical label-free methods can be divided into two main categories, reflectometric and refractometric [6].

In reflectometric sensors, the transducer consists of layers with different refractive index, to which a layer of dielectric material and the layer of recognition molecules are included. The most common reflectometric sensing method is the one known as reflectometric interference spectroscopy (RIfS), introduced by Gauglitz et al. in 1991 [7]. The RIfS transducer is, usually, a glass slide modified with a thin layer of transparent dielectric material (e.g.,  $\text{SiO}_2$ ,  $\text{SiO}_2\text{-Ta}_2\text{O}_5$ ) on top of which the specific recognition molecules are immobilized. When white light strikes the glass substrate from the backside, the partial beams are reflected at each interface, interfere, and create a reflectance spectrum with alternating maxima and minima corresponding to constructive and destructive interference of the reflected radiation. Binding reactions taking place on top of the dielectric layer increase the optical path length, causing a shift in the reflectance spectrum, which is proportional to the thickness increase and consequently to the concentration of the reacting molecules. Over the years, several variations of the initial biosensing method have been presented, in which the white light source and whole reflection spectrum recording were replaced by light sources with a narrow spectral width, enabling multiplex detection in microtiter plates or sensor arrays [8,9], as well as single-wavelength light set-ups suitable for imaging [10]. Moreover, apart from glass, other materials have been investigated as substrates, including porous silicon as is or in combination with dielectric materials [11,12]. White Light Reflectance Spectroscopy (WLRS) is another label-free reflectometric detection method based on the reflection of a white light beam from a silicon chip surface with a dielectric layer on top that has been engineered so that the reflected spectrum to have at least an interference fringe in the visible spectrum [13]. This sensing approach has been applied over the years for the determination of either single or multiple analytes, related to human disease diagnostics or food safety, using the same optical set-up; the latter was possible through appropriate engineering of the chip [14]. Moreover, effort was devoted to the automation of the assay and signal processing, aiming towards the development of a small-sized device for on-site determinations [15].

Refractometric transducers rely on another transduction principle, that of evanescent field optics. The evanescent field is generated by the electromagnetic field of the light as it transverses a waveguide by means of total internal reflection. The main characteristic of this field is that it extends to a depth ranging from a few tens to a few hundreds of nanometers, depending on the waveguide material and geometry, and its intensity is exponentially reduced as the distance from the waveguide increases. Nonetheless, the evanescent field is very sensitive to changes in the refractive index on the waveguide surface and can thus “sense” the interaction between molecules immobilized onto the waveguide surface with their counterpart molecules. The change in the thickness of the biomolecular layer influences the evanescent field and its coupling back into the waveguide, causing a change in the intensity, polarity, or phase of the waveguided light. The major categories of refractometric sensors include surface plasmon resonance (SPR), grating coupler, photonic crystal, ring resonator, and interferometric sensors (Figure 1).

Surface plasmon resonance (SPR) is the most widely explored label-free optical detection principle [16]. SPR biosensors are based on the immobilization of the recognition molecule on top of a gold layer deposited on a prism, a grating coupler, or a dielectric waveguide. Light that passes from these components and strikes the gold layer at a certain angle can excite the free conducting electrons (plasmons) of the metal and create a surface plasmon wave at the solution/gold interface. This wave is very sensitive to refractive index changes at the gold layer surface, and as a result, the angle of incident light has to change during the course of a binding reaction to preserve the surface plasmon wave. Thus, it is possible to monitor in real time binding reactions, by monitoring the incident light resonance angle. Despite the fact that SPR has found numerous applications in diverse fields and a few companies have commercialized devices based on this transduction principle,

the need for external optical components has restricted their miniaturization and confined the use of SPR instruments in the lab. A way to surpass these limitations is offered by the localized SPR or LSPR transduction approach, in which the continuous metal layer has been replaced by metallic nanostructures (nanospheres, nanorods, or nanodisks) of sub-wavelength size [2]. The light that strikes the nanostructures excites the metal free electrons and when resonance is achieved, certain wavelengths are scattered from the nanostructures. Thus, binding reactions can be monitored in real time as shifts in the resonance wavelength. Regarding the question about which format, the classical SPR or LSPR, is more sensitive, the literature reports show that SPR might be more sensitive than LSPR in terms of bulk refractive index changes, while LSPR might be equally sensitive to changes that occur in close proximity to the surface, and therefore more suitable for the monitoring of biomolecular interactions [17].

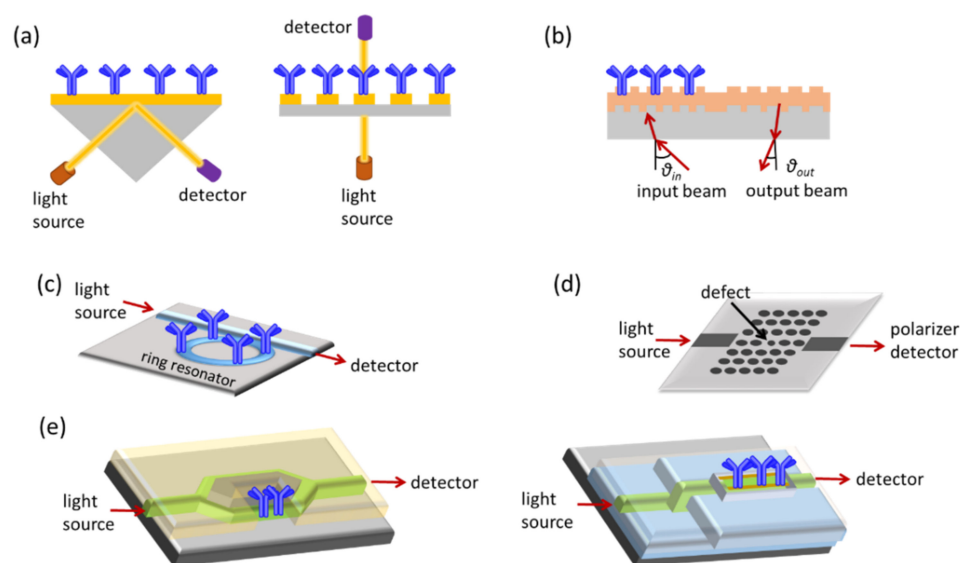


**Figure 1.** Schematic presentation of label-free optical sensing methods: (a) SPR, (b) grating couplers, (c) ring resonators, (d) photonic crystals, and (e) interferometers.

Nevertheless, the analytical performance is one only of the parameters that should be taken into consideration when the application of a sensing system outside a laboratory environment is sought [18]. To this end, the simplicity of the measurement procedure (ideally, the user should only load the sample), the cost-effectiveness in terms of both the instrumentation and the consumables required, and the ability to work with complex matrices, but, most importantly, the potential for miniaturization are of utmost importance. Thus, sensors based on integrated optics can be more easily downsized, integrated with external optical components, and interconnected with fluidic and electronic modules, and therefore are the most promising candidates for incorporation into portable devices. Other advantages of integrated optical sensors are the high versatility of materials and technologies available for their fabrication and the ability to create arrays of sensors suitable for multiplex determinations [19]. Although polymers have been implemented as substrates for the fabrication of integrated optical devices, silicon remains the material of choice for high-performance optical devices. A short description of the detection principles of the different integrated optical sensor categories is provided below.

## 2. Integrated Optical Sensors

In grating coupler sensors, the transducer is a planar waveguide with a grating on its surface, i.e., a periodic pattern, to enable light in-coupling and transmission along the waveguide. The light coupling is sensitive to changes in the refractive index of the medium over the waveguide, allowing monitoring of binding reactions occurring onto the waveguide surface by monitoring the incident light in-coupling angle. Moreover, the

interaction of the biomolecular layer with the waveguided photons through the evanescent wave field makes it possible to monitor its building-up by monitoring changes in the light out-coupling angle. This latter configuration is advantageous compared to the first one because there is no need for precision alignment of the light to the grating, thus leading to simpler experimental set-ups [20]. Moreover, several improvements regarding the light in- and out-coupling onto the waveguide allowed multi-analyte determinations using arrays of grating coupler-based sensors [21].

Ring resonators combine a linear waveguide with a circular one in which the light propagating through the linear one is coupled through the evanescent wave field and propagates in the form of whispering-gallery modes. Changes in the refractive index on the ring surface change the spectral position of the whispering-gallery modes and thus resonance is achieved at a different wavelength of the incident light. The fact that the light propagating in the ring interacts multiple times with the molecules on its surface makes ring resonators considerably more sensitive than linear waveguides of the same length. Sensitivity is also enhanced when, instead of a 2D format (microdisk or microring), the resonator acquires a 3D format (microtoroid) [22].

Another category of integrated optical sensors is those based on photonic crystals, i.e., periodical nanostructures on a crystal, which allows the propagation of selected wavelengths of the incident light. If a “defect” is introduced in the periodic structure, the propagation of light is accomplished only when resonance is achieved. As this resonance is influenced by refractive index changes around the defect area, label-free monitoring of bioreactions taking place on the photonic crystal surface is possible. The most popular photonic crystal sensor configuration is a waveguide with arrays of holes arranged in lines or hexagonal lattices on which the defect is created either by missing holes in the pattern or by changing the spacing or size of the holes at some point of the waveguide [23]. In general, photonic crystal sensors are less sensitive compared to other types of integrated optical transducers.

Integrated interferometers could attain several configurations, the most popular of which are Mach–Zehnder (MZI), Young (YI), or bimodal interferometers (BI). Integrated MZIs are linear waveguides that at some point split into two arms, the sensing and the reference, that recombine to a single waveguide after a certain distance. The whole structure is covered by a cladding layer, except from a part of the sensing arm, the sensing window, that is modified with the binding molecules. When a biomolecular interaction takes place on the sensing window, the associated change in the refractive index induces a phase difference between the light that propagates into the sensing arm to that propagating into the reference ones. Thus, the output light intensity has a cosine dependence to the input light. Consequently, MZIs are more sensitive when they operate away from the extrema of the interference spectrum, where the “sensitivity” in refractive index changes is almost negligible. The analytical performance of sensors based on MZIs depends on the sensing arm interaction length, the geometrical characteristics of the waveguide (symmetric MZI with equal lengths of the sensing and the reference arm or asymmetric), and the difference in the refractive index of the waveguide (e.g., glass, SiO<sub>2</sub>, Si<sub>3</sub>N<sub>4</sub>, polymer) and cladding layer material (usually SiO<sub>2</sub>) [24,25]. The majority of MZI-based instruments employ monochromatic light sources, i.e., lasers; nonetheless, to reduce the size and complexity of instrumentation, broadband light sources have been also explored instead of lasers. These light sources can be external [26] or integrated to the same substrate with the transducers [27]. The latter will be further discussed in the following section.

Young interferometers also comprise a waveguide that splits into two arms, which, however, in contrast to MZIs, do not converge on the chip but the two light beams interfere in free space, creating an “interferogram” that can be depicted on a CCD camera [28]. Although there is theoretical and experimental evidence that YIs can be more sensitive for a particular application than sensors based on SPR, grating couplers, or reflectometric interference spectroscopy (RIFS) [28], there are very few reports of biosensors based on YIs in the literature compared to other integrated optical transducers.

Bimodal interferometers represent a category of interferometric sensors that relies on a single waveguide with two different light propagation zones. The first zone supports a single mode and the second two modes (zero- and first-order modes). This means that refractive index changes occurring at the waveguide surface, i.e., due to a biomolecular reaction, effect a change in the interference pattern recorded at the waveguide output since the propagation velocity of two modes depends on the refractive index of the medium on top of the waveguide [29]. Bimodal interferometers have comparable analytical performance to single-wavelength MZIs and in addition have the potential of multiplexed determinations and integration into small-sized instruments [29].

Prior to delving further into monolithically integrated optical sensors, the principles of immunochemical detection methods will be briefly discussed.

### 3. Principles of Immunochemical Detection Methods

The widespread use of antibodies as recognition elements in biosensors results from their high selectivity and sensitivity but also from the fact they have been used for years in standard immunochemical detection methods, as are the enzyme immunoassays performed on microtiter plates (i.e., ELISAs). Thus, although, in principle, some optical transduction techniques have the necessary sensitivity to monitor directly the antigen–antibody binding, in many cases, this ability is limited to high-molecular-weight analytes, the binding of which can cause a substantial change in sensor response. Therefore, the assay formats usually applied in microtiter plate immunoassays are also employed in immunosensors, namely the competitive and the non-competitive assay format (Figure 2).

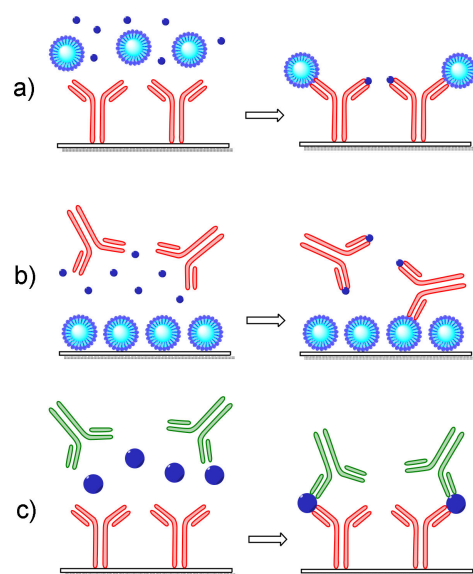


**Figure 2.** Schematic presentation of different assay formats applied to optical immunosensors: (a) a competitive immunoassay with the antibody immobilized onto the transducer, (b) a competitive immunoassay with the antigen immobilized onto the transducer in form of a protein conjugate, and (c) a non-competitive immunoassay employing a pair of antibodies, one immobilized onto the transducer and the other for detection of analyte molecules bound onto the immobilized antibody.

Non-competitive immunoassays are better suited for low-molecular-weight analytes such as toxins, pesticides, antibiotics, pharmaceutical residues, etc. There are two general approaches based on immobilization onto the transducer surface of either the antigen-specific antibody (Figure 2a) or the antigen itself (Figure 2b). In the first approach, the antigen concentration in the samples is determined through its competition with an antigen bound onto a carrier (usually selected to enhance the sensor signal) for coverage to the immobilized antibody binding sites. In the second approach, the transducer is modified with the antigen either directly or in the form of an antigen–protein conjugate. Again, deter-

mination of the antigen concentration in a sample is realized through its competition with the surface-bound antigen for coverage of the antibody binding sites. In both approaches, the signal recorded in the transducer is inversely proportional to the antigen concentration in the sample; thus, the highest signal is received in the absence of the antigen (zero calibrator). Both of the above-described approaches can be applied for an antigen–antibody pair; nonetheless, the second might be preferable when the stability of the immobilized biomolecule is considered since low-molecular-weight antigens or their protein conjugates are less prone to loss of functionality compared to antibodies.

The non-competitive or sandwich immunoassay format is usually followed when the antigen has at least two antigenic determinants or epitopes in its molecule since it requires the combination of two antibodies that do not compete with each other for binding to the antigen. Thus, to perform a non-competitive immunoassay (Figure 2c), one of the antibodies should be immobilized onto the transducer surface (capture antibody) and a second one (detection or reporter antibody) is attached on a different epitope of the surface-bound antigen molecules, forming a “sandwich”. In sensors based on label-free transduction principles, the detection antibody might be non-labeled; however, the use of labeled antibodies is possible even in these cases, aiming at the enhancement of the signal derived by the binding of the detection antibody, and consequently the analytical sensitivity of the assay, i.e., the lowest antigen concentration that can be determined.

#### 4. Monolithically Integrated Interferometric Transducers

As discussed in Section 2, the majority of the integrated optical sensors, including the interferometric ones, relied on external monochromatic light sources, i.e., lasers. Due to the low light coupling efficiency to the waveguides, lasers with high intensity of emitted light had to be implemented, which were bulky and energy-demanding. Thus, it was almost impossible to build portable systems based on these components. To reduce the instrumentation size, broadband light sources were coupled to integrated MZIs in an attempt to realize sensors suitable for on-site determinations [30,31]. An external spectrum analyzer working in the 1200–1700 nm spectral region was employed to record the output light. Although the detection sensitivities achieved with these sensors were lower compared to those implementing monochromatic light sources, the use of a broadband light source solved the phase ambiguity issue of monochromatic MZI, which arises from the fact that information might be lost if the refractive index changes resulted in phase shifts equal to or multiple-times equal to  $2\pi$ . Introduction of an on-chip optical spectral analyzer along with an array of MZIs and a grating for broadband light in-coupling improved the sensor performance [26,32]. Thus, a limit of detection (LOD) of  $6 \times 10^{-6}$  RIU in terms of refractive index was achieved, which was comparable to the LODs of monochromatic MZIs. Broadband light sources have been also combined with integrated Young interferometers, for which it was predicted by simulations that the implementation of these light sources would enable discrimination between refractive index changes caused by binding reactions rather than medium changes [33]. These theoretical predictions have not been proved experimentally so far.

In all efforts mentioned, the light source, either monochromatic or broadband, was external, and additional optical components, lenses, gratings, etc., were required to couple the light onto the integrated waveguides. The way to extract light from silicon has been known since the 1960s [34]; however, the low intensity of these light sources, combined with the difficulty to efficiently couple this light to waveguides made onto the same substrate, prohibited their implementation in biosensing devices for almost 50 years. Then, a new approach to monolithically integrate silicon waveguides, light sources, and detectors into the same silicon substrate was introduced [35]. The integrated light source was a silicon avalanche diode (LED), which emitted light covering all the visible and near-infrared spectrum when reversed-biased beyond its breakdown point. The realization of working sensors based on silicon components all fabricated onto the same substrate required inventive solutions of two problems, the bending of the waveguides towards the

LED and the photodetector to avoid light losses, and the alignment of the LED with the waveguide. The process followed to solve these two problems is summarized in Figure 3. Thus, at first, a 2- $\mu\text{m}$ -thick thermally grown silicon dioxide layer was deposited on the silicon substrate, on which the positions of the LED and photodetector were defined through photolithography and etching of the silicon dioxide layer. To these openings, the base of the avalanche junction ( $\text{N}^+$ ) and the p/n junction at the photodetector side were formed by phosphorus implantation (Figure 3i). Then, an additional 2- $\mu\text{m}$ -thick silicon dioxide layer was created by deposition of tetraethyl orthosilicate (TEOS) (Figure 3ii). The TEOS layer was etched in  $\text{CHF}_3$  plasma to create curvatures towards the LED and photodetector side (Figure 3iii). Low-pressure chemical vapor deposition (LPCVD) of a silicon nitride film with a thickness of around 150 nm was then performed using a mixture of  $\text{NH}_3$  and  $\text{SiH}_2\text{Cl}_2$  (Figure 3iv). Photolithography and etching in  $\text{CHF}_3$  plasma were applied again to create the strip waveguides, one end of which was just above the avalanche diode base area. Following this, the avalanche diode was created by boron implantation through the nitride film, which acted as a mask guiding the formation of the LED immediately under the up-going segment of the waveguide (Figure 3v). Finally, the silicon dioxide cladding layer was formed by deposition, and etched above the waveguides to define the sensing windows. This process resulted in less than 1-micron misalignment of the LED with respect to waveguide and a light coupling efficiency that reached almost 40% [35].

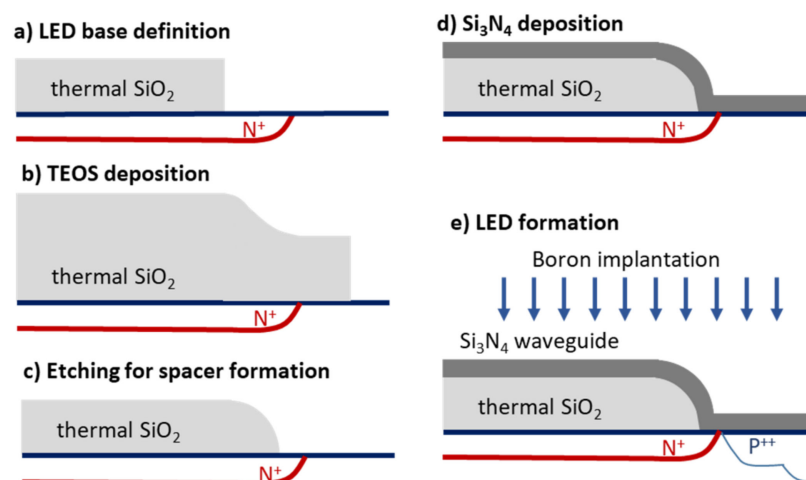


**Figure 3.** Schematic of the process followed for integrated transducer fabrication: (a) formation of avalanche diode base, (b) silicon dioxide deposition, (c) plasma etching for bending spacer creation (d), deposition of silicon nitride film and waveguide patterning, and (e) boron implantation through the silicon nitride film for self-aligned formation of the LED.

In the first version of monolithically integrated silicon optical sensors, the LEDs were coupled to linear silicon nitride waveguides and signal transduction was based on monitoring the drop in the intensity of light transmitted through the waveguide and recorded by the photodetector due to its interaction with light-absorbing labels attached to targeted analytes [35,36]. Nonetheless, shortly after, the linear waveguides were replaced by MZIs, ten of which were arranged in a fan-like way on a single chip, each one connected to its own integrated LED and all of them converging to the same output point [27,37,38]. Moreover, to ensure that the light transmitted was monomodal, a mode filter was introduced prior to the waveguide. It was theoretically and experimentally shown using these chips that broadband Mach–Zehnder interferometry could surpass both the phase ambiguity and signal fading of standard single-wavelength MZIs [27,37,38]. This was ascribed to the fact that a given change in the refractive index of the medium above the sensing waveguide window corresponds to a different phase shift for each wavelength, and thus minute changes in the refractive index could be detected more accurately by processing the full transmission spectrum rather than monitoring a single wavelength.

Two configurations of the integrated MZIs have been realized, a fully (Figure 4a) and a semi-integrated one (Figure 4b). The former incorporated on a single chip, along with the integrated LEDs and the MZIs, as a detector, an integrated photodiode and had an LOD in terms of refractive index of  $1 \times 10^{-5}$  RIU. This configuration was applied to monitor binding reactions, including the interaction of immobilized biotin with streptavidin and mouse IgG with an anti-mouse IgG antibody, with LODs of 1 nM and 10 nM for streptavidin and anti-mouse IgG, respectively [37]. Despite the promising analytical results, it was obvious that the fully integrated version suffered from the limitation of phase ambiguity and signal fading of the monochromatic MZIs since the use of a photodetector for signal collection suppressed the information available in the spectrum to a single value. Thus, the semi-integrated version that employed an external spectrophotometer for recording the transmission spectrum was further exploited as an immunosensor [38–44]. The spectrum recorded contained two characteristic frequencies, one for the TE and one for the TM mode, which could be discriminated through Fourier transform, offering the ability to monitor binding events by monitoring either of them without significant effects on the analytical performance. The analytical sensitivity of the semi-integrated device, with respect to the bulk refractive index, was determined at  $5 \times 10^{-6}$  RIU. For the binding assays of biotinylated bovine serum albumin with streptavidin and anti-mouse IgG with mouse IgG, LODs of 5 pM and 32 pM, respectively, were determined, demonstrating the considerably higher detection sensitivity of the semi-integrated configuration as compared to the fully integrated one [38].

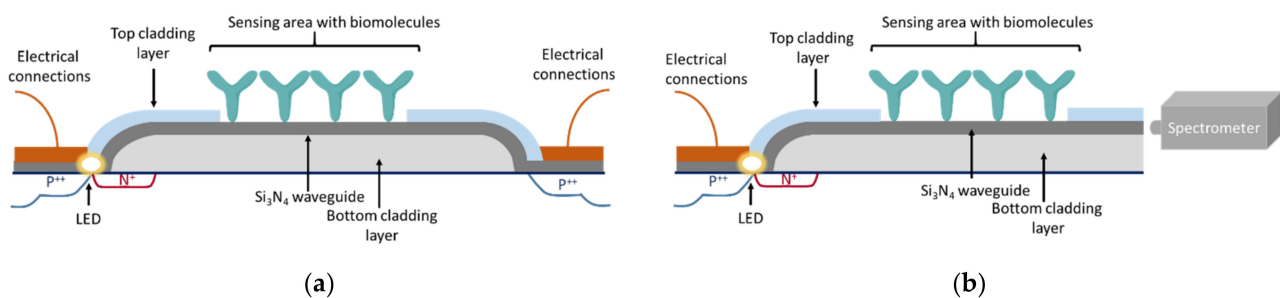


**Figure 4.** Cross-section depiction of fully integrated (a) and the semi-integrated (b) broadband MZI configuration.

Thus, the semi-integrated configuration was implemented in both single- and multi-analyte immunochemical determinations. The first application related to the detection of goat milk adulteration with bovine milk through the immunochemical determination of bovine k-casein [39]. A competitive immunoassay was developed using MZIs modified with bovine k-casein and a specific antibody against this protein. The LOD of the assay was 0.04% (*v/v*) bovine in goat milk and the assay's dynamic range was from 0.1 to 1.0% (*v/v*). Moreover, the assay was completed in 10 min. The same assay format and reagents were applied to detect mozzarella or feta adulteration with bovine cheese [40]. In this case also, the assay duration was less than 10 min and the limit of quantification for bovine cheese in mozzarella and feta cheese was 0.5 and 0.25% (*w/w*), respectively—well below the maximum allowable content of bovine milk in mozzarella and feta (1% *w/w*) according to the EU regulations. The mycotoxin ochratoxin A was also detected in beer samples following a competitive immunoassay format. The assay detection limit was 2.0 ng/mL and its dynamic range 4.0–100 ng/mL [41]. The high detection sensitivity of integrated MZI-based immunosensors allowed the determination of C-reactive protein (CRP), a widely used inflammation marker, in human serum samples in approximately 5 min by monitoring the direct binding of the analyte to an antibody immobilized onto the windows of the MZIs' sensing arms [42]. A quantification limit of 4.2 ng/mL was achieved, allowing an at least 100-times dilution of the serum that alleviated any matrix effect onto the sensor response. In addition, the CRP concentrations determined in human serum samples with the sensor

were in excellent agreement with those determined for the same samples by a clinical analyzer, supporting the accuracy of the measurements performed with the sensor.

The realization of arrays of 10 integrated MZIs on a single chip (with dimensions  $4.25 \times 8.0 = 34 \text{ cm}^2$ ) offered the possibility for multiplexed determinations through modification of the sensing arms' window areas of different MZIs with different binding molecules. Thus, by immobilizing protein conjugates of three mycotoxins, each one on three MZIs of the chip, and leaving the last one for the determination of the non-specific binding signal, the simultaneous determination of aflatoxin B1, fumonisin B1, and deoxynivalenol in beer samples was accomplished following a competitive immunoassay format. The assays' LODs were 0.8, 5.6, and 24 ng/mL for aflatoxin B1, fumonisin B1, and deoxynivalenol, respectively, and the overall assay duration was only 12 min [43]. Analysis of different types of beers produced around the world showed that the sensor could perform as well as established instrumental laboratory methods [44]. Following a similar procedure, the simultaneous detection of four allergens, bovine milk protein, peanut protein, soy protein, and gliadin, was demonstrated [45]. In this case, the four allergenic proteins were immobilized onto the integrated MZIs to perform a competitive immunoassay that was completed in 6.5 min, providing LODs of 0.04, 1.0, 0.80, and 0.10  $\mu\text{g/mL}$ , for bovine milk protein, peanut protein, soy protein, and gliadin, respectively. Evaluation of sensor performance through the analysis of samples from the cleaning-in-place system of a dairy facility showed that the results obtained with the sensor were in good agreement with those acquired by commercial ELISAs for the determination of each antigen separately.

The use of integrated silicon LEDs as light sources for interferometric sensors was expanded to integrated YIs [46]. Similarly to MZIs, it was shown that the implementation of a polychromatic light source led to an interferogram consisting of two distinct fringe packets, one for each polarization, making feasible the independent determination of the phase signal for the two polarizations. The sensor was evaluated using the binding reactions of streptavidin and anti-mouse IgG antibody with immobilized biotin and mouse IgG, respectively. Using a concentration of streptavidin of 1 nM and anti-rabbit IgG of 10 nM, peak shifts of more than one period were observed, indicating that LODs down to the sub-nM range could be achieved [47]. Nonetheless, the preliminary experiments revealed also the weak points of the set-up and especially the need for precise alignment of the chip with respect to the CCD array used to record the signal. Therefore, further advancements regarding the experimental set-up are required in order to benefit in full from the analytical performance of the integrated YIs.

The need for external detectors, especially in the case of integrated MZIs where a spectrophotometer was required, compromised the portability potential offered by the small chip size. Thus, a spectrum analyzer and a photodiode array were integrated into the chip with the 10 integrated MZIs and the ultimate degree of integration of all passive and active components on a single chip was achieved without increasing considerably the overall chip size ( $37 \text{ mm}^2$ ). Based on these chips, a portable instrument was manufactured that encompassed in a  $21 \times 17 \times 7 \text{ cm}^3$  case the chip docking station, a micropump for reagent circulation, and the electronics for turning on the light sources sequentially and recording the signal from the 10 MZIs. The sensor provided an LOD of 60 pM for a direct binding assay of anti-mouse IgG antibody onto immobilized mouse IgG and 8 pM for a non-competitive immunoassay of C-reactive protein, both completed in around 10 min. The good analytical performance of these integrated sensors and the small chip and instrumentation size are the main pros of this approach, promoting the application of the sensor and instrument at the point-of-need. Regarding the cons of this approach, one can consider the high complexity of chip fabrication and the associated cost, and the need for the more automated handling of the reagents required to perform the assay.

## 5. Conclusions and Outlook

From the information provided in the previous sections, it is obvious that monolithically integrated optical transducers demonstrate excellent analytical performance in

different application fields, ranging from biodiagnostics to environmental monitoring and food safety. Moreover, these transducers seem to provide a viable solution towards the development of portable systems that could be used for analysis outside the analytical laboratory, i.e., at the point-of-need. Towards this goal, an additional advantage of monolithically integrated optical sensors is the fact that they are fabricated with techniques compatible with large-scale production at a reasonable cost. Despite the fact that the research efforts described have resulted in prototypes that work efficiently in a laboratory environment, there are still different aspects to be addressed prior to moving these prototypes to the point-of-need. As mentioned, such a limiting factor is the handling of the sample and, in general, of solutions required for assay performance, which could employ several reaction steps. To this end, a new sensing approach has been exploited in which, contrary to the previous efforts, only the MZIs are integrated onto the chip in such a way that allows the coupling of both the input and output light from the same side of the chip. In the other side of the chip the sensing windows of the MZIs are located, which, after appropriate modification with biomolecules, will allow the monitoring of binding reactions by simple dipping onto solutions, thus abolishing the need for fluidics and fluid manipulation. Provided that the new approach demonstrates the analytical performance of former monolithically integrated optical sensors, it will be the ideal solution for on-site, rapid analytical determinations of high accuracy.

**Author Contributions:** P.P., E.M., I.R., S.K. and K.M. contributed to the manuscript equally. All authors have read and agreed to the published version of the manuscript.

**Funding:** This research received no external funding.

**Institutional Review Board Statement:** Not applicable.

**Informed Consent Statement:** Not applicable.

**Data Availability Statement:** No new data were created or analyzed in this study. Data sharing is not applicable to this article.

**Conflicts of Interest:** The authors declare no conflict of interest.

## References

1. Clark, L., Jr.; Lyons, C. Electrode systems for continuous monitoring in cardiovascular surgery. *Ann. N. Y. Acad. Sci.* **1962**, *102*, 29–45. [[CrossRef](#)] [[PubMed](#)]
2. Vashist, S.K.; Lippa, P.B.; Yeo, L.Y.; Ozcan, A.; Luong, J.H.T. Emerging technologies for next-generation point-of-care testing. *Trend Biotechnol.* **2015**, *33*, 692–705. [[CrossRef](#)]
3. Lopez, G.A.; Estevez, M.-C.; Solera, M.; Lechuga, L.M. Recent advances in nanoplasmonic biosensors: Applications and lab-on-a-chip integration. *Nanophotonics* **2017**, *6*, 123–136. [[CrossRef](#)]
4. Makarona, E.; Petrou, P.; Kakabakos, S.; Misiakos, K.; Raptis, I. Point-of-Need bioanalytics based on planar optical interferometry. *Biotechnol. Adv.* **2016**, *34*, 209–233. [[CrossRef](#)] [[PubMed](#)]
5. Walt, D.R. Optical methods for single molecule detection and analysis. *Anal. Chem.* **2013**, *85*, 1258–1263. [[CrossRef](#)] [[PubMed](#)]
6. Gauglitz, G. Direct optical detection in bioanalysis: An update. *Anal. Bioanal. Chem.* **2010**, *398*, 2363–2372. [[CrossRef](#)] [[PubMed](#)]
7. Gauglitz, G.; Nahm, W. Observation of spectral interferences for the determination of volume and surface effects of thin films. *Fresenius J. Anal. Chem.* **1991**, *341*, 279–283. [[CrossRef](#)]
8. Rothmund, M.; Schütz, A.; Brecht, A.; Gauglitz, G.; Berthel, G.; Gräfe, D. Label free binding assay with spectroscopic detection for pharmaceutical screening. *Fresenius J. Anal. Chem.* **1997**, *359*, 15–22. [[CrossRef](#)]
9. Gauglitz, G. Multiple reflectance interference spectroscopy measurements made in parallel for binding studies. *Rev. Sci. Instr.* **2005**, *76*, 062224. [[CrossRef](#)]
10. Bleher, O.; Schindler, A.; Yin, M.-X.; Holmes, A.B.; Lippa, P.B.; Gauglitz, G.; Proll, G. Development of a new parallelized, optical biosensor platform for label-free detection of autoimmunity-related antibodies. *Anal. Bioanal. Chem.* **2014**, *406*, 3305–3314. [[CrossRef](#)]
11. Arshavsky-Graham, S.; Massad-Ivanir, N.; Segal, E.; Weiss, S. Porous silicon-based photonic biosensors: Current status and emerging applications. *Anal. Chem.* **2019**, *91*, 441–467. [[CrossRef](#)] [[PubMed](#)]
12. Chen, Y.; Liu, J.; Yang, Z.; Wilkinson, J.S.; Zhou, X. Optical biosensors based on refractometric sensing schemes: A review. *Biosens. Bioelectron.* **2019**, *144*, 111693. [[CrossRef](#)] [[PubMed](#)]
13. Koukouvinos, G.; Petrou, P.; Goustouridis, D.; Misiakos, K.; Kakabakos, S.; Raptis, I. Development and bioanalytical applications of a white light reflectance spectroscopy label-free sensing platform. *Biosensors* **2017**, *7*, 46. [[CrossRef](#)] [[PubMed](#)]

14. Anastasiadis, V.; Koukouvinos, G.; Petrou, P.S.; Economou, A.; Dekker, J.; Harjanne, M.; Heimala, P.; Goustouridis, D.; Raptis, I.; Kakabakos, S.E. Multiplexed mycotoxins determination employing white light reflectance spectroscopy and silicon chips with silicon oxide areas of different thickness. *Biosens. Bioelectron.* **2020**, *153*, 112035. [[CrossRef](#)]
15. Tsounidi, D.; Koukouvinos, G.; Christianidis, V.; Legaki, E.; Giogli, V.; Panagiotopoulou, K.; Taka, S.; Ekaterinidi, Z.; Kakabakos, S.; Raptis, I.; et al. Development of a point-of-care system based on white light reflectance spectroscopy: Application in CRP determination. *Biosensors* **2021**, *11*, 268. [[CrossRef](#)]
16. Yesudasu, V.; Pradhan, H.S.; Pandya, R.J. Recent progress in surface plasmon resonance based sensors: A comprehensive review. *Heliyon* **2021**, *7*, e06321. [[CrossRef](#)]
17. Mazzotta, F.; Johnson, T.W.; Dahlin, A.B.; Shaver, J.; Oh, S.-H.; Höök, F. Influence of the evanescent field decay length on the sensitivity of plasmonic nanodisks and nanoholes. *ACS Photonics* **2015**, *2*, 256–262. [[CrossRef](#)]
18. Zanchetta, G.; Lanfranco, R.; Giavazzi, F.; Bellini, T.; Buscaglia, M. Emerging applications of label-free optical biosensors. *Nanophotonics* **2017**, *6*, 627–645. [[CrossRef](#)]
19. Estevez, M.-C.; Alvarez, M.; Lechuga, L.M. Integrated optical devices for lab-on-a-chip biosensing applications. *Laser Photon. Rev.* **2011**, *6*, 1–25. [[CrossRef](#)]
20. Lukosz, W.; Clerc, D.; Nellen, P.M.; Stamm, C.; Weiss, P. Output grating couplers on planar optical waveguides as direct immunosensors. *Biosens. Bioelectron.* **1991**, *6*, 227–232. [[CrossRef](#)]
21. Kehl, F.; Etlinger, G.; Gartmann, T.E.; Tschamer, N.S.R.U.; Heub, S.; Follonier, S. Introduction of an angle interrogated, MEMS-based, optical waveguide grating system for label-free biosensing. *Sens. Actuator B* **2016**, *226*, 135–143. [[CrossRef](#)]
22. Zhang, X.M.; Choi, H.S.; Armani, A.M. Ultimate quality factor of silica microtoroid resonant cavities. *Appl. Phys. Lett.* **2010**, *96*, 153304. [[CrossRef](#)]
23. Dorfner, D.; Zabel, T.; Hurlimann, T.; Hauke, N.; Frandsen, L.; Rant, U.; Abstreiter, G.; Finley, J. Photonic crystal nanostructures for optical biosensing applications. *Biosens. Bioelectron.* **2009**, *24*, 3688–3692. [[CrossRef](#)] [[PubMed](#)]
24. Sarkar, D.; Gunda, N.S.K.; Jamal, I.; Mitra, S.K. Optical biosensors with an integrated Mach-Zehnder Interferometer for detection of *Listeria monocytogenes*. *Biomed. Microdev.* **2014**, *16*, 509–520. [[CrossRef](#)] [[PubMed](#)]
25. Chalyan, T.; Guider, R.; Pasquardini, L.; Zanetti, M.; Falke, F.; Schreuder, E.; Heideman, R.G.; Pederzoli, C.; Pavesi, L. Asymmetric Mach-Zehnder interferometer based biosensors for aflatoxin M1 detection. *Biosensors* **2016**, *6*, 1. [[CrossRef](#)] [[PubMed](#)]
26. Martens, D.; Ramirez-Priego, P.; Murib, M.S.; Elamin, A.A.; Gonzalez-Guerrero, A.B.; Stehr, M.; Jonas, F.; Anton, B.; Hlawatsch, N.; Soetaert, P.; et al. A low-cost integrated biosensing platform based on SiN nanophotonics for biomarker detection in urine. *Anal. Method.* **2018**, *10*, 3066–3073. [[CrossRef](#)]
27. Misiakos, K.; Raptis, I.; Salapatras, A.; Makarona, E.; Botsialas, A.; Hoekman, M.; Stoffer, R.; Jobst, G. Broad-band Mach-Zehnder interferometers as high performance refractive index sensors: Theory and monolithic implementation. *Opt. Exp.* **2014**, *22*, 8856–8870. [[CrossRef](#)]
28. Ymeti, A.; Greve, J.; Lambeck, P.V.; Wijn, R.; Heideman, R.G.; Kanger, J.S. Drift correction in a multichannel integrated optical Young interferometer. *Appl. Opt.* **2005**, *44*, 3409–3412. [[CrossRef](#)]
29. Zinoviev, K.E.; Gonzalez-Guerrero, A.B.; Dominguez, C.; Lechuga, L.M. Integrated bimodal waveguide interferometric biosensor for label-free analysis. *J. Lightwave Technol.* **2011**, *29*, 1926–1930. [[CrossRef](#)]
30. Luo, D.H.; Levy, R.A.; Hor, Y.F.; Federici, J.F.; Pafchek, R.M. An integrated photonic sensor for in situ monitoring of hazardous organics. *Sens. Actuator B* **2003**, *92*, 121–126. [[CrossRef](#)]
31. Li, Y.; Harris, E.; Chen, L.; Bao, X. Application of spectrum differential integration method in an in-line fiber Mach-Zehnder refractive index sensor. *Opt. Express* **2010**, *18*, 8135–8143. [[CrossRef](#)] [[PubMed](#)]
32. Mulder, H.K.P.; Ymeti, A.; Subramaniam, V.; Kanger, J.S. Size-selective detection in integrated optical interferometric biosensors. *Opt. Exp.* **2012**, *20*, 20934. [[CrossRef](#)] [[PubMed](#)]
33. Nagata, T.; Namba, T.; Kuroda, Y.; Miyake, K.; Miyamoto, T.; Yokoyama, S.; Miyazaki, S.; Koyanagi, M.; Hirose, M. Single-chip integration of light-emitting diode, waveguide and micromirrors. *Jpn. J. Appl. Phys.* **1995**, *34*, 1282–1285. [[CrossRef](#)]
34. Chynoweth, A.G.; McKay, K.G. Photon emission from avalanche breakdown in silicon. *Phys. Rev.* **1956**, *102*, 369–376. [[CrossRef](#)]
35. Misiakos, K.; Kakabakos, S.E.; Petrou, P.S.; Ruf, H.H. A monolithic silicon optoelectronic transducer as a real-time affinity biosensor. *Anal. Chem.* **2004**, *76*, 1366–1373. [[CrossRef](#)]
36. Misiakos, K.; Petrou, P.S.; Kakabakos, S.E.; Yannoukakos, D.; Contopanagos, H.; Knoll, T.; Velten, T.; DeFazio, M.; Schiavo, L.; Passamano, M.; et al. Fully integrated monolithic optoelectronic transducer for real-time protein and DNA detection: The NEMOSLAB approach. *Biosens. Bioelectron.* **2010**, *26*, 1528–1535. [[CrossRef](#)]
37. Misiakos, K.; Raptis, I.; Makarona, E.; Botsialas, A.; Salapatras, A.; Oikonomou, P.; Psarouli, A.; Petrou, P.S.; Kakabakos, S.E.; Tukkineni, K.; et al. All-silicon monolithic Mach-Zehnder interferometer as a refractive index and biochemical sensor. *Opt. Exp.* **2014**, *22*, 26803–26813. [[CrossRef](#)]
38. Psarouli, A.; Salapatras, A.; Botsialas, A.; Petrou, P.S.; Raptis, I.; Makarona, E.; Jobst, G.; Tukkineni, K.; Sopanen, M.; Stoffer, R.; et al. Monolithically integrated broad-band Mach-Zehnder interferometers for highly sensitive label-free detection of biomolecules through dual polarization optics. *Sci. Rep.* **2015**, *5*, 17600. [[CrossRef](#)]
39. Angelopoulou, M.; Botsialas, A.; Salapatras, A.; Petrou, P.S.; Haasnoot, W.; Makarona, E.; Jobst, G.; Goustouridis, D.; Siafaka-Kapadai, A.; Raptis, I.; et al. Assessment of goat milk adulteration with a label-free monolithically integrated optoelectronic biosensor. *Anal. Bioanal. Chem.* **2015**, *407*, 3995–4004. [[CrossRef](#)]

40. Angelopoulou, M.; Petrou, P.S.; Raptis, I.; Misiakos, K.; Livaniou, E.; Makarona, E.; Kakabakos, S.E. Rapid detection of mozzarella and feta cheese adulteration with cow milk through a silicon photonic immunosensor. *Analyst* **2021**, *146*, 529–537. [[CrossRef](#)]
41. Pagkali, V.; Petrou, P.S.; Salapatias, A.; Makarona, E.; Peters, J.; Haasnoot, W.; Jobst, G.; Economou, A.; Misiakos, K.; Raptis, I.; et al. Detection of ochratoxin A in beer samples with a label-free monolithically integrated optoelectronic biosensor. *J. Hazard. Mater.* **2017**, *323*, 75–83. [[CrossRef](#)] [[PubMed](#)]
42. Psarouli, A.; Botsialas, A.; Salapatias, A.; Stefanitsis, G.; Nikita, D.; Jobst, G.; Chaniotakis, N.; Goustouridis, D.; Makarona, E.; Petrou, P.S.; et al. Fast label-free detection of C-reactive protein using broad-band Mach Zehnder interferometers integrated on silicon chips. *Talanta* **2017**, *165*, 458–465. [[CrossRef](#)] [[PubMed](#)]
43. Pagkali, V.; Petrou, P.S.; Makarona, E.; Peters, J.; Haasnoot, W.; Jobst, G.; Moser, I.; Gajos, K.; Budkowski, A.; Economou, A.; et al. Simultaneous determination of aflatoxin B1, fumonisin B1 and deoxynivalenol in beer samples with a label-free monolithically integrated optoelectronic biosensor. *J. Hazard. Mater.* **2018**, *359*, 445–453. [[CrossRef](#)] [[PubMed](#)]
44. Angelopoulou, M.; Petrou, P.S.; Makarona, E.; Haasnoot, W.; Moser, I.; Jobst, G.; Goustouridis, D.; Lees, M.; Kalatzi, K.; Raptis, I.; et al. Ultrafast multiplexed-allergen detection through advanced fluidic design and monolithic interferometric silicon chips. *Anal. Chem.* **2018**, *90*, 9559–9567. [[CrossRef](#)]
45. Makarona, E.; Salapatias, A.; Raptis, I.; Petrou, P.; Kakabakos, S.; Stavra, E.; Malainou, A.; Misiakos, K. Broadband Young interferometry for simultaneous dual polarization bioanalytics. *J. Opt. Soc. Am. B Opt. Phys.* **2017**, *34*, 1691–1698. [[CrossRef](#)]
46. Savra, E.; Malainou, A.; Salapatias, A.; Botsialas, A.; Petrou, P.; Raptis, I.; Makarona, E.; Kakabakos, S.E.; Misiakos, K. Monolithically-integrated Young interferometers for label-free and multiplexed detection of biomolecules. *Proc. SPIE* **2016**, *9752*, 97520N.
47. Misiakos, K.; Makarona, E.; Hoekman, M.; Fyrogenis, R.; Tukkiniemi, K.; Jobst, G.; Petrou, P.S.; Kakabakos, S.E.; Salapatias, A.; Goustouridis, D.; et al. All-silicon spectrally resolved interferometric circuit for multiplexed diagnostics: A monolithic Lab-on-a-Chip integrating all active and passive components. *ACS Photonic* **2019**, *6*, 1694–1705. [[CrossRef](#)]